



## Brain grey matter perfusion in primary progressive multiple sclerosis: Mild decrease over years and regional associations with cognition and hand function

Benoit Testud, Clara Delacour, Ahmed Ali El Ahmadi, Gilles Brun, Nadine Girard, Guillaume Duhamel, Christoph Heesen, Vivien Häussler, Christian Thaler, Arzu Ceylan Has Silemek, et al.

### ► To cite this version:

Benoit Testud, Clara Delacour, Ahmed Ali El Ahmadi, Gilles Brun, Nadine Girard, et al.. Brain grey matter perfusion in primary progressive multiple sclerosis: Mild decrease over years and regional associations with cognition and hand function. European Journal of Neurology, 2022, 10.1111/ene.15289 . hal-03594256

HAL Id: hal-03594256

<https://amu.hal.science/hal-03594256>

Submitted on 14 Nov 2022

**HAL** is a multi-disciplinary open access archive for the deposit and dissemination of scientific research documents, whether they are published or not. The documents may come from teaching and research institutions in France or abroad, or from public or private research centers.

L'archive ouverte pluridisciplinaire **HAL**, est destinée au dépôt et à la diffusion de documents scientifiques de niveau recherche, publiés ou non, émanant des établissements d'enseignement et de recherche français ou étrangers, des laboratoires publics ou privés.



Distributed under a Creative Commons Attribution - NonCommercial 4.0 International License

# Respiratory-triggered quantitative MR spectroscopy of the human cervical spinal cord at 7 T

Tangi Roussel<sup>a,b,\*</sup>, Yann Le Fur<sup>a,b</sup>, Maxime Guye<sup>a,b</sup>, Patrick Viout<sup>a,b</sup>, Jean-Philippe Ranjeva<sup>a,b</sup>, Virginie Callot<sup>a,b</sup>

<sup>a</sup>Aix Marseille Univ, CNRS, CRMBM, Marseille, France

<sup>b</sup>APHM, Hôpital Universitaire Timone, CEMEREM, Marseille, France

---

## Abstract

**Purpose:** Ultra-high field <sup>1</sup>H MR spectroscopy (MRS) is of great interest to help characterizing human spinal cord pathologies. However, very few studies have been reported so far in this small size structure at these fields due to challenging experimental difficulties caused by static and radiofrequency field heterogeneities, as well as physiological motion. In this work, in line with recent developments proposed to strengthen spinal cord MRS feasibility at 7 T, a respiratory-triggered acquisition approach was optimized to compensate for dynamic B<sub>0</sub> field heterogeneities and to provide robust cervical spinal cord MRS data.

**Methods:** A semi-LASER sequence was purposely used, and a dedicated raw data processing algorithm was developed to enhance MR spectral quality by discarding corrupted scans. To legitimate the choices done during the optimization stage, additional tests were carried out to determine the impact of breathing, voluntary motion, body mass index and fitting algorithm. An in-house quantification tool was concomitantly designed for accurate estimation of the metabolite concentration ratios for choline, N-acetyl-aspartate, myo-inositol and glutathione. The method was tested on a cohort of 14 healthy volunteers.

**Results:** Average water linewidth and NAA signal-to-noise ratio reached 0.04 ppm and 11.01, respectively. The group-average metabolic ratios were in good agreement with previous studies and showed inter-session reproducibility variations below 30%.

**Conclusion:** The developed approach allows a rise of the acquired MRS signal quality and of the quantification robustness as compared to previous studies hence offering strengthened possibilities to probe the metabolism of degenerative and traumatic spinal cord pathologies.

**Keywords:** human spinal cord, MR spectroscopy, ultra-high field, quantification

---

\*Corresponding author  
Email address: [tangi.roussel@univ-amu.fr](mailto:tangi.roussel@univ-amu.fr) (Tangi Roussel)

5510 words

## Introduction

While  $^1\text{H}$  magnetic resonance spectroscopy (MRS) can provide a unique window into the central nervous system metabolism in a non-invasive way, spinal cord  $^1\text{H}$  MRS is of particular interest in the study of several degenerative and traumatic pathologies [1]. Previous reports at 3 T have shown altered metabolic profiles when probing spinal cord of patients with multiple sclerosis [2], amyotrophic lateral sclerosis [3] or spinal cord injury [4]. Among these metabolic profiles, a drop of N-acetyl-aspartate (NAA), considered as a robust marker of neuronal integrity and function, coupled with an increase in myo-inositol (mI), a glial cell marker, are for example commonly observed [1].  $^1\text{H}$  MRS may therefore help to characterize inflammatory and/or neurodegenerative processes occurring within the spinal cord in these various diseases and provide complementary and specific information about metabolism which cannot be obtained otherwise.

Numerous experimental difficulties make the use of single-voxel MRS challenging in the case of this particular organ [5]. The volume of interest (VOI) is often below 1 cm $^3$  due to the small cross-sectional dimensions of the spinal cord [1] while it ranges from 1 to 10 cm $^3$  in the brain [6]. To compensate the subsequent loss in signal-to-noise ratio (SNR), the number of averages collected are increased at the expense of scan time, making spinal cord MRS a time-consuming modality and therefore prone to subject motion and thus severe signal loss. Besides subject motion, physiological motion such as cerebrospinal fluid (CSF) pulsations introduces phase distortion errors during MRI acquisitions [7]. Electrocardiogram (ECG)-triggering is therefore strongly suggested when performing spinal cord imaging or spectroscopy [8].

Concurrently, ultra-high field (UHF  $\geq 7$  T) MRI has been a major breakthrough and advantages have been demonstrated in a variety of MR acquisition modalities, including MRS [9, 10].  $^1\text{H}$  UHF-MRS studies have been therefore conducted in the brain [11, 12] but also in the spinal cord using dedicated cervical radio-frequency (RF) coils [13]. More than half of the studies related to spinal cord exploration at 7 T were focused on RF coil design or involved an aspect of coil design [14]. Indeed, the  $B_1$  field heterogeneities encountered at UHF are substantially larger than at lower fields and, in the case of the spinal cord, are exacerbated by the presence of vertebral bodies [14]. To compensate for these inhomogeneities, adiabatic RF pulses are increasingly employed at UHF for magnetization inversion and spatial selection [15, 16] at the expense of specific absorption rate (SAR).

A further major challenge in UHF spinal cord exploration is the presence of severe  $B_0$  field inhomogeneities [14, 11]. Originating from magnetic susceptibility differences between the various type of tissues and bones present near the spinal cord, these static field heterogeneities are increased as compared to 3 T. Moreover, it was shown that subject breathing causes dynamic  $B_0$  field changes in the brain [17] and even stronger periodic  $B_0$  field fluctuations in the spinal cord during MRI at 7 T [18]. The authors suggested that these variations originate from air/tissue magnetic susceptibility differences and that the periodic changes in lung volume during respiration cause “the  $B_0$  field to vary periodically with the respiratory cycle, even at some distance from the chest”. As magnetic susceptibility effects increase linearly with  $B_0$  [10], these field distortions are further amplified at UHF.

In this context and in line with developments to strengthen  $^1\text{H}$  spinal cord MRS feasibility [19, 13],

the objectives of this work were: (i) to evaluate the exact impact of physiological motion and especially breathing on the acquired spinal cord MRS data at 7 T; (ii) to consequently design a 7 T-dedicated protocol for quantitative  $^1\text{H}$  spinal cord MRS that compensates for dynamic  $B_0$  field heterogeneities based on a respiratory-triggered semi-LASER acquisition approach, and (iii) to develop an original and fully-automatic post-processing method to reconstruct the data allowing SNR and resolution improvement by discarding compromised data. Quantitative estimation of metabolic profiles over 14 healthy subjects are finally reported followed by reproducibility results to show potential of such breathing-compensated MRS approach. Note that the brain MRS recommendations recently published by an international group of MRS experts [6, 20, 21, 22] were followed whenever possible and adapted for the spinal cord exploration.

## Method

Acquisitions were performed on a 7-T system (MAGNETOM Step 2, Siemens Healthcare, Erlangen, Germany) equipped with a 70-mT/m SC-72 gradient system. Spinal cord MRS was conducted using a 8-channel RF transmit/receive neck coil array (Rapid Biomedical, Rimpar, Germany). A volume transceiver / 32-channel receiver head coil (Nova Medical Inc, Wilmington, MA, USA) was used for additional brain MRS tests.

## Subjects

The study was approved by the local ethics committee and written consents were obtained from all participants prior to MR examinations. Spinal cord MRS acquisitions were performed on 14 healthy

subjects (4 males and 10 females, mean age  $28.3 \pm 4.7$  years old). Cardiac pulsation and respiration were monitored using a finger pulse oximeter sensor and an elastic bellow belt (Siemens part #4752882) placed on the abdomen, respectively. When performing acquisition tests related to breathing, the recorded physiological traces were saved for later use. Seven of the 14 subjects were rescanned 6 months later for reproducibility purposes. Brain MRS acquisitions were also carried out on 3 healthy subjects (1 male and 2 females, mean age  $30.3 \pm 0.6$  years old).

## MRI acquisitions

Spinal cord anatomical MRI consisted of a 3-plane gradient-echo (GE) localizer (TE/TR= 4.0/8.6 ms,  $1.2 \times 1.2 \text{ mm}^2$  in-plane resolution, 5 slices, 5 mm slice thickness, TA= 30s) and a pulse oximeter -triggered sagittal multi-slice  $T_2$ -weighted imaging scan (TE/TR= 22/4000 ms,  $1.5 \times 0.8 \text{ mm}^2$  in-plane resolution, 10 slices, 2.2 mm slice thickness, TA= 3min 20s). Standard  $B_0$  field homogenization was carried using a 3D slab containing the neck. The VOI for the MRS acquisition was positioned at the C3 cervical level, its dimensions and orientation were adjusted to avoid any CSF contamination. The average voxel dimensions in the RL, AP and HF dimensions were 6.95 mm, 6.50 mm and 21.05 mm, respectively (Fig. 1C).  $B_1$  voltage calibration was performed using a variable flip-angle single-voxel localized sequence [23].

## MRS acquisitions

Single-voxel MRS was performed using a semi-LASER sequence [16]. Sequence parameters such as gradient spoilers, RF excitation and refocusing pulses

were optimized on a home-made multi-compartment brain metabolite phantom to maximize SNR and spatial selectivity while minimizing TE. Substantial improvements were achieved by adjusting specifically the adiabatic full passage (AFP) refocusing RF pulses' duration and adiabaticity parameters, i.e. the time-bandwidth-product ( $R$ ) and the hyperbolic secant order (HSn) (results not shown here). The maximum RF voltage achievable by the RF coil, the SAR and thus the achievable minimum TR were also taken into account and two main semi-LASER protocols were set-up according to the  $B_1$  configuration: (i) a strong- $B_1$  protocol (#1) with adiabatic refocusing RF pulses (9 ms,  $R=20\text{-}30$ , HSn=1) for high spatial selectivity and SNR and (ii) a low- $B_1$  protocol (#2) (4 ms,  $R=10$ , HSn=2), which offers a good compromise between SNR/TE and spatial selectivity. Note that protocol (#1) was always preferred over protocol (#2). Whenever needed, TR was increased to satisfy SAR limits. However, when protocol (#1) resulted in a TR above 5s because of SAR limitations, protocol (#2) was performed instead to maintain theoretical scan time below 10min. For both protocols, a 2-ms excitation RF pulse and a 1-ms 40-mT/m gradient spoiler were employed. 64 to 128 averages were collected from an average  $0.97 \pm 0.36$  mL voxel placed in the spinal cord at the C3 vertebral level (Fig. 1). The echo time was always set to minimum resulting in an average TE of 46.01 ms.

Water suppression (WS) was performed using VAPOR [24] and was not fully optimized to maintain a relatively intense water peak residue in the acquired MR spectra. Non-water-suppressed (noWS) MRS scans were also acquired (8 averages). All MRS scans were performed with 4 dummy scans and 80-mm outer volume suppression (OVS) bands. The transmit RF frequency offset was set to -1.7 and

0 ppm relative to water for WS and noWS acquisitions, respectively.

As recently recommended for brain MRS [6, 20],  $B_0$  field homogenization was systematically performed using the FASTESTMAP sequence (4 echoes, the acquisition delay “Tau” was adjusted to maintain the intensity of the last echo above 25% of the intensity of the first echo) [25]. To maximize the chances of reaching a global minimum, the operator followed a 2-step shimming routine: (i) a first stage dedicated to first-order shimming (“Linear 6-proj”), with 2 to 3 iterations in order to converge to a first set of optimal shim currents, followed by (ii) a second stage as an attempt for second-order shimming (“Full 6-proj”). After each iteration, the water peak FWHM was estimated. Any FWHM increase during this iterative process indicated that the  $B_0$  field homogenization failed; in that case, the last set of optimal shim currents was restored.

Finally, all voxel-localized MRS acquisitions were respiratory-triggered and set to occur during the expiratory phase. Each respiratory cycle allowed the acquisition of one single average or individual spectrum. The semi-LASER sequence preparation (c.a. 760 ms), the echo time (46 ms in average) and the acquisition (with a signal duration of c.a. 100 ms) were all taking place during the expiratory pause, between two respirations (Fig. S6, see section F of the supplementary information). Similar to previous reports [26], the respiratory trigger of the FASTESTMAP acquisitions was delayed by 760 ms, corresponding to the total preparation time of the semi-LASER sequence.

## Additional experiments

### Breathing MRS tests

Using the same VOI as for MRS scans, additional acquisitions were performed on 4 healthy subjects to evaluate the influence of respiration on the recorded MRS signal. Similar to the procedure described in [18], these additional experiments consisted in acquiring repeatedly the water MR spectrum, without any triggering, while asking the subject to breathe normally or to hold his/her breath in inspiration for 10s. To detect any breathing-induced effects, the time resolution was maximized and TR was thus minimized. Consequently, because of the long TRs obtained with the semi-LASER sequence, a non water-suppressed STEAM sequence was employed with a TR of 900 ms during 2 minutes without any triggering ( $TE/TM = 3.5/8.1$  ms). The respiration signal was recorded and stored for later use.

### Brain MRS tests

Inversion recovery (IR) semi-LASER acquisitions were performed to evaluate the presence and potentially model the macromolecular spectral baseline [21, 22]. However, IR-MRS experiments are prone to very low SNR and require substantial acquisition times. Making the simplistic assumption that the macromolecular baseline distribution is similar in the brain and in the spinal cord, these experiments were thus carried out in the brain on one subject using the protocol described above. The VOI was placed in the corona radiata brain area and its volume was adjusted to 3.38 mL (Fig. 1B), which is a relatively small volume according to literature [6]. 128 averages were collected using an inversion time of 950 ms [27, 28] (see section C in the supplementary infor-

mation for details). Non-IR brain MRS acquisitions were additionally carried out on 3 healthy subjects to qualitatively compare MR spectra and general data quality with datasets acquired on spinal cord.

### Data processing

The raw MRS data were post-processed using an in-house Python 3.7 software made open-source and publicly available (<https://crmbm.univ-amu.fr/softwares/pastis>). The signal processing included: channel-by-channel phasing, channel combination using single value decomposition (SVD), zero-filling and average-by-average frequency realignment. First-order phasing and channel combination were performed by estimating the signal phase and amplitude from the corresponding noWS dataset allowing the compensation of eddy current effects. SNR values were all calculated following LCModel's SNR definition [29] as the ratio of the intensity of the NAA singlet at 2.01 ppm to the standard deviation (SD) of noise in the [-2:-1] ppm range multiplied by a 0.5-factor. If not explicitly stated otherwise, FWHM values were estimated on the residual water peak at 4.7 ppm on WS MRS data.

Data processing included a specific routine to improve spectral quality by discarding corrupted data: individual acquired MR spectra were extracted from frequency-realigned raw data and automatically analyzed by estimating the amplitude, the FWHM, the chemical shift and phase variations of the residual water peak at 4.7 ppm in frequency domain according to the acquisition time. An algorithm was developed to analyze the 4 latter peak properties time evolutions and to automatically adjust thresholds to discard individual MR spectra. To do so, an optimal range of thresholds in terms of peak amplitude,

FWHM, chemical shift and phase to test were generated by sorting the measurements and removing duplicates in order to reduce computation time. For each set of thresholds, individual MR spectra whose peak properties exceeded thresholds were discarded and the final averaged and frequency-realigned spectrum was calculated. The optimal set of thresholds was estimated to either (i) increase the final SNR (of at least 1%) if possible while maintaining or reducing final peak FWHM or (ii) reduce final FWHM when no SNR gain was possible. The optimal set of thresholds was generated for each acquired dataset and the computation time for this process was less than 30s per dataset (8x1.9 GHz processor). To evaluate this approach, all acquired MR data were processed with and without data discard.

Finally, the raw data obtained from non-triggered non-water-suppressed STEAM experiments under normal breathing and breath-hold were analyzed in terms of water peak amplitude, FWHM, chemical shift and phase but no data was discarded. Instead, the FWHM and chemical shift variations were compared in time- and frequency-domain to the respiration signal recorded from the bellow belt.

## Data quantification

The developed in-house Python software described above also allows data quantification. The fitting algorithm design is similar to QUEST [30] and operates in complex time-domain. The model consists of a linear combination of  $M$  metabolite time MRS signals numerically computed using the pyGAMMA library [31] with ideal RF pulses and relies on the following equation:

$$\hat{x}(t) = \sum_{m=1}^M c_m \cdot \hat{x}(t)^m \cdot \exp [(\Delta\alpha_m + i \cdot \Delta\omega_m) \cdot t + i \cdot \phi_{0m}]$$

where  $c_m$  is the relative concentration of the simulated metabolite signal  $\hat{x}(t)^m$ ,  $\Delta\alpha_m = \frac{1}{T_{2m}^*}$  is the damping factor [Hz],  $\Delta\omega_m$  is the frequency shift [Hz] and  $\phi_{0m}$  is the zero-order phase [rad]. The fitting model was implemented to be dynamically-adjustable, meaning that any fitting parameter can be linked to one or more parameters. The latter allowed the model simplification to  $(2 \cdot M + 2)$  parameters by assuming a global phase shift for all metabolites. Three consecutive numerical optimizations with decreasing fit parameter ranges and constraints were performed using a Jacobian-matrix-driven least-square algorithm (*scipy* Python package). The developed fitting algorithm allowed the estimation of Cramér-Rao lower bounds (CRB) for each estimated metabolite. Note that the noise level estimation required for the CRB calculation was systematically performed on raw MRS data and without any apodization. Unlike the original QUEST algorithm, no special handling of the macromolecular background signal using the initial time points was performed [30]. Additionally and for comparison purposes, all datasets were quantified with LCModel [32] (see section E of the supplementary information).

The metabolite basis sets were computed for each acquired dataset depending on its TE and included 10 metabolites: creatine (Cr), glutamate (Glu), glutamine (Gln), glutathione (GSH), glycerophosphocholine (GPC), myo-inositol (mI), N-acetyl aspartate (NAA), N-acetyl aspartate glutamate (NAAG), phosphocholine (PC) and phosphocreatine (PCr). The total choline (tCho), total creatine (tCr) and total NAA

(tNAA) concentrations were computed by summing the concentration estimates from GPC and PC, Cr and PCr, NAA and NAAG, respectively. Any water peak residue or lipid resonances in the chemical shift ranges of [4.3; 6] ppm and [0; 1.8] ppm were removed before quantification by Hankel singular value decomposition (HSVD). Three gaussian components were added to the metabolite basis set at 0.9, 1.3 and 1.6 ppm respectively to fit any residual lipid resonances. The estimated metabolite concentrations were corrected for  $T_2$  relaxation effects; metabolite  $T_2$  relaxation times were extracted from literature [33, 34, 35, 36, 12].  $T_1$  relaxation effects were neglected and thus not corrected because of the long TR set during the acquisition.

Before computing the final quantification results at group level, some datasets were excluded from the group based on MRS data and fit quality parameters. As recommended in the literature [37, 21], CRB were not employed as a rejection criterion but rather as an indicator to discuss the validity of the estimations. Instead, any datasets with a SNR below an arbitrary threshold of 6, or a water FWHM above 20 Hz [20], or a fit quality number (FQN) [21] above 10, were rejected. The FQN was calculated as the ratio of the variance of the fit residue spectrum in the [0; 4.2] ppm range to the variance of the spectral noise in the [-2; 0] ppm range. Finally, average and SD metabolite concentration ratios relative to tCr were computed. To evaluate the reproducibility of the method, the coefficient of variation (COV) (SD/mean expressed in %) was calculated using the data collected in two separate scan sessions separated of 6 months for n= 4 healthy subjects.

## Results

### Non-triggered spinal cord MRS and dynamic fluctuations with respiration

During non-triggered MRS acquisitions, the water resonance was impacted by periodic variations of linewidth and chemical shift (Fig. 2A, B, D). The water resonance variations and the respiration signal were compared in frequency-domain (Fig. 2C, E) and showed for both of them a peak for ca. 13 beats per minute (BPM), which was actually the subject breathing rate. Similarly, non-triggered MRS acquisitions during subject breath-hold showed strong changes in linewidth and chemical shift (Fig. S1, see section A.1 in the supplementary information).

### Data processing and threshold-based data discard

Fig. 3 shows the graphical output of the data discard step during the data processing for subject S11. The water resonance residue that remained after non-optimal WS was analyzed in each individual acquired spectrum. The peak intensity, FWHM, frequency and phase shift were plotted in time (Fig. 3A, B, C and D). The algorithm previously described automatically adjusted thresholds for each peak property (Fig. 3B, red horizontal lines) and the corresponding excluded individual spectra were discarded from the final MRS data reconstruction (Fig. 3, red spectra). In the case of a subject motion (Fig. S2), this approach could also allow the detection and the discard of corrupted acquired data (see section A.2 in the supplementary information). At a group level, this approach led to an average data discard rate of 5.9 %. Interestingly, these data were discarded mainly because of excessive water FWHM (42% of

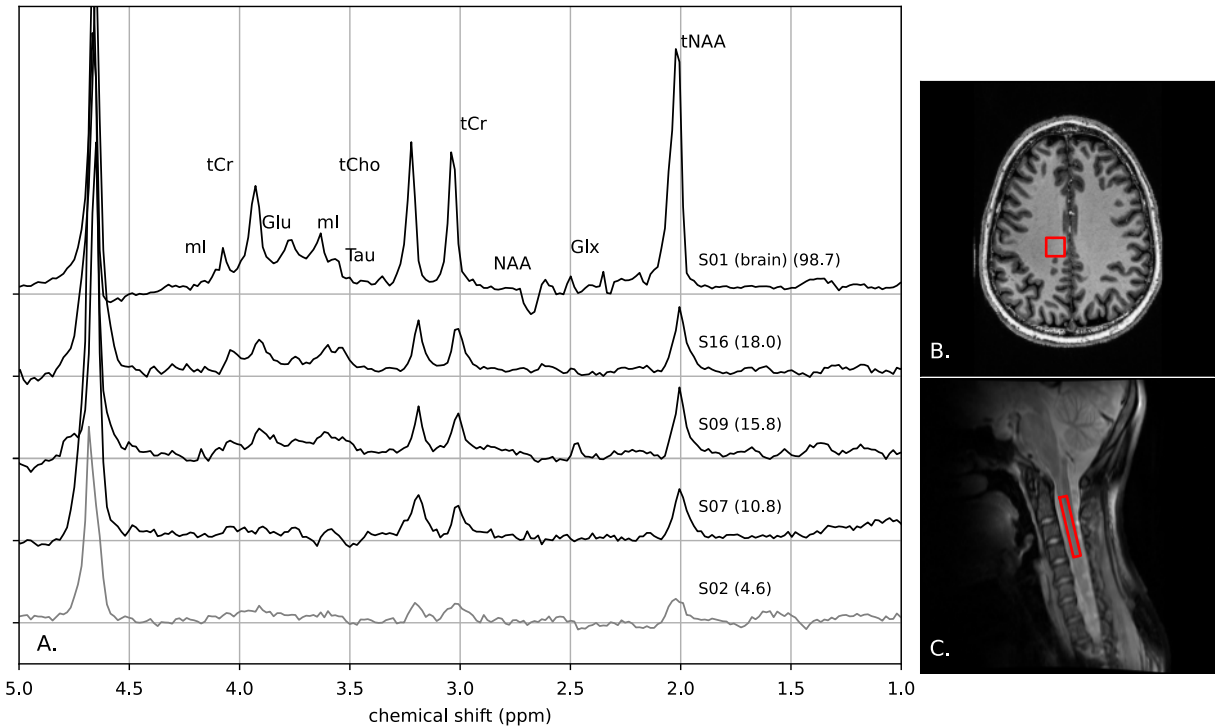


**Figure 1:** One brain and 4 spinal cord semi-LASER MRS datasets acquired from subjects S01, S02, S07, S09 and S16 at 7 T (A). For each spectrum, the SNR estimated on the NAA peak is indicated. The brain VOI (subject S01, 15 mm x 15 mm x 15 mm voxel size) was placed using T<sub>1</sub>-weighted brain images (B). T<sub>2</sub>-weighted spinal cord images (C) were employed to place the VOI at the C3 vertebral level (here, subject S09, 6 mm x 6 mm x 20 mm or 0.72 mL voxel size). Substantial MRS data quality differences were observed between brain and spinal cord MR signals: while coupled metabolites resonances are clearly visible in the brain MRS spectrum at c.a. 2.5 ppm, they show very low intensity, if not near noise level, in spinal cord acquired spectra. The latter reflects mainly the significantly larger VOI volumes available for brain MRS acquisition (3.38 mL here) compared to spinal cord ( $0.97 \pm 0.36$  mL). The MR spectrum acquired on subject S02 (gray) was excluded from the group because of poor quality (SNR < 6).

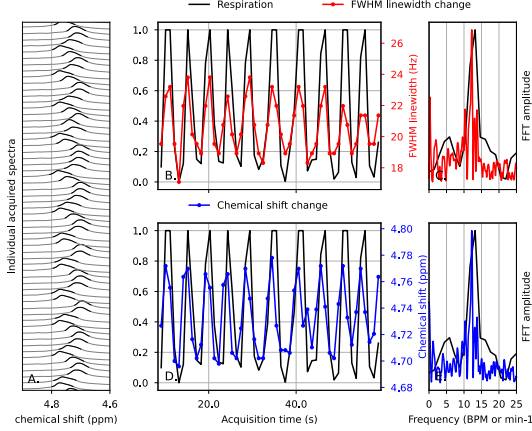


**Figure 2:** Results of a 2-min non-water-suppressed STEAM acquisition (subject S10) without respiratory-triggered (TR = 900 ms). The subject was asked to breathe normally. For each individual spectrum (A), the water peak FWHM (B, red) and chemical shift (D, blue) were evaluated. A clear correlation in time- (B, D) and in frequency-domain (C, E) with the respiration signal (black) is shown with a maximum at 13 BPM (respiration period= 4.6s).

the cases). Excessive phase, chemical shift and amplitude changes affected 25, 17 and 17% of the datasets, respectively.

### Spectral quality and SNR

An overview of the general spectral quality encountered in this study after data processing is shown in Fig. 1 and 4. For each subject, the quality of the acquired MRS data was evaluated in terms of SNR and water FWHM. Over 20 datasets (14 baseline and 6 reproducibility), 4 datasets were discarded from the study based on SNR, FWHM and FQN thresholds (Fig. 4). In other words, 80% of the acquired spinal cord MRS datasets were successfully included in the study. The average SNR and residual water FWHM were  $11.01 \pm 3.88$  and  $12.59 \pm 2.55$  Hz ( $0.04 \pm 0.01$  ppm), respectively. The average wa-

ter FWHM estimated on noWS MRS datasets was  $13.19 \pm 3.32$  Hz ( $0.04 \pm 0.01$  ppm). The SNR estimated on brain MRS datasets acquired using the same protocol (with the larger VOI volume) were c.a. 10 times higher. Overall, on the spinal cord, the average TE was  $46.01 \pm 13.51$  [21.16; 90.00]. The strong- $B_1$  protocol (#1) led to a substantially shorter TE compared to the default low- $B_1$  protocol (#2) with an average TE of  $33.08 \pm 6.73$  and  $51.55 \pm 11.79$  ms, respectively. The average voxel dimensions and chemical shift displacement errors (CSDE) along the RL, AP and HF directions were of 6.95, 6.50, 21.05 mm and 11.42, 11.49, 12.90 %/ppm, respectively. The latter resulted in an average voxel displacement along the RL, AP and HF directions of 0.80 mm, 0.76 mm and 2.70 mm for the NAA resonance and of 1.35 mm, 1.29 mm and 4.59 mm for the residual water resonance. Given its HF dimension, the VOI covered the whole C3 level but also partially the C2 and C4 levels (Fig. 1). While the prescribed acquisition time based on nominal TR was in average less than 10min, the effective acquisition time reached an average of 13min likely due to respiratory-triggering and breathing instabilities.

As SNR depends in general on VOI size and number of averages, the normalized SNR, i.e. normalized by the number of averages and the VOI volume, was calculated for all datasets and then compared to body mass index (BMI) and voxel depth (distance between RF coil and VOI) to investigate the potential relationship with data quality (see section B and Fig. S3 of supplementary information). The BMI group average was found equal to  $20.56 \pm 2.89$  kg/m<sup>2</sup> (median = 20.55) and a normalized SNR dependence with the subject BMI and voxel depth was observed ( $R=0.65$ ).

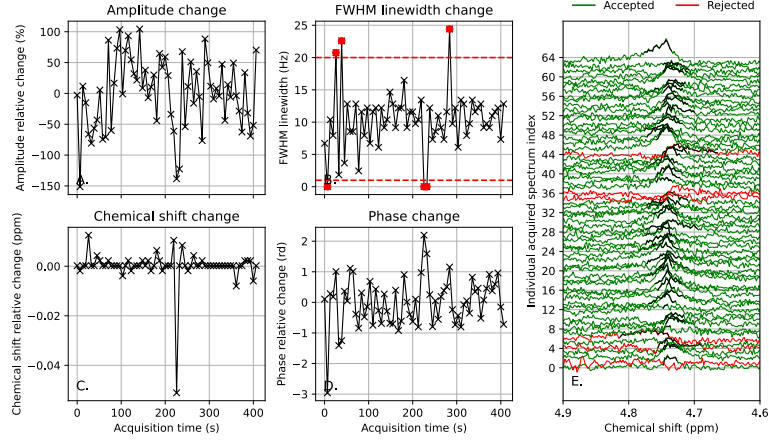


**Figure 3:** Data discard stage of a spinal cord MRS single-voxel acquisition (subject S11). Individual spectra were extracted from raw data (E); the residual water peak was analyzed in terms of amplitude (A), linewidth (B), chemical shift (C) and phase variations (D). A number of individual acquisitions were rejected (E) according to thresholds adjusted by the algorithm (B, red horizontal lines). In this case, the data rejection algorithm found that discarding data based on the FWHM criterion gave the highest gain in SNR and/or FWHM. Six individual acquisitions out of 64 were discarded (E, in red) because the linewidth was above 20 Hz (automatically adjusted threshold) or below 1 Hz (residual water peak not detected) as illustrated in (B). This data processing allowed a final SNR increase by 4.80%.

### Second order shimming and spectral artifacts

As described above, first and second order  $B_0$  field homogenization was attempted. In average, the water FWHM increased by  $10.17 \pm 9.81$  Hz when attempting second order shimming. Water FWHM was improved (decreased) for only 3 subjects. Interestingly, when second order  $B_0$  field homogenization failed (increased water FWHM), this led to severe spectral artifacts (Fig. S5, see section D of the supplementary information).

### Data quantification

The IR semi-LASER acquisitions performed on brain revealed very low intensity macromolecular resonances at TE=40 ms (Fig. S4). Considering the low SNR of the acquired MRS data on spinal cord compared to brain (c.a. 10-fold factor) and the po-

tential differences in macromolecular profile between those two organs, the modelization of these resonances was neglected except for three lipid resonances below 2 ppm.

The processed MRS data were given as an input to the fitting algorithm. Fig. 5 shows an example of fitting of a spinal cord MR spectrum. The average FQN was  $2.96 \pm 1.19$ . In general, the fitting procedure took less than 30s (using a 8x1.9 GHz processor with 16 Gb memory). Mean, SD, average CRB and COV were computed for each metabolite concentration ratios (Table 1). Results were finally compared to spinal cord quantitative MRS reports in literature in Table 2. Additional quantification results obtained with LCModel were reported as well for comparison (see Table S1).

	With data discard			Without data discard		
	Ratio (SD)	CRB (%)	COV (%)	Ratio (SD)	CRB (%)	COV (%)
Gln	0.72 (0.52) *	60.01	140.48	0.75 (0.75)	170.18	89.17
Glu	0.55 (0.52) *	114.70	91.66	0.69 (0.96)	543.71	78.81
GSH	0.38 (0.29)	38.03	29.56	0.34 (0.32)	575.42	35.71
mI	1.18 (0.31)	35.72	21.88	1.25 (0.48)	28.91	18.48
tCho	0.35 (0.11)	45.55	13.21	0.38 (0.19)	47.44	15.33
tNAA	1.21 (0.22)	36.64	10.24	1.27 (0.46)	30.41	11.81

**Table 1:** Quantification results for n = 12 healthy subjects. For each metabolite, the average and SD concentration ratio relative to tCr, the corresponding mean CRB and coefficient of variation (COV) over 4 subjects and 2 time-points were computed. Two MRS data reconstruction approaches were considered: with and without data discard. Metabolite quantification results marked with a (\*) showed a high CRB and/or COV and were therefore excluded.

Study	Current	Henning et al. [13]	Hock et al. [38]	Marliani et al. [39]
B <sub>0</sub>	7 T	7 T	3 T	3 T
Sequence	Respiratory-triggered semi-LASER	ECG-triggered semi-LASER	ECG-triggered MC-PRESS	PRESS
Cervical level	C3	C2-C3	C3-C4	C2-C3
TE	46 ±13 ms	43 ms	30 ms	35 ms
NA	64-128	128	128 *	128
Scan time	13min	7.5min	>5.3min *	14min
SNR	11.29 ±3.85	7.6	8.5 *	4
FWHM	0.04 ±0.01 ppm	0.09 ppm	0.07 ppm *	0.10 ppm
Subjects	12	7	7	13
tCho	0.35 (0.11)	0.32 (0.20)	0.52 (0.15) *	0.5 (0.1)
tNAA	1.21 (0.22)	1.31 (0.20)	1.59 (0.20) *	1.4 (0.3)
mI	1.18 (0.31)	1.08 (0.22)	1.34 (0.19) *	1.7 (0.2)
GSH	0.38 (0.29)	-	0.46 (0.26) * **	-

**Table 2:** Comparative table summarizing spinal cord MRS quantification results available in the literature. For each study, the average and inter-subject SD metabolite concentration ratios are given. Additionally, the B<sub>0</sub> field, the MRS sequence along with the main acquisition parameters, the average SNR and FWHM obtained and the number of subjects are detailed. Values marked with a (\*) were extracted from the results labeled “128 echoes” published in [38]. GSH ratios marked with a (\*\*) included ascorbate concentration estimates.

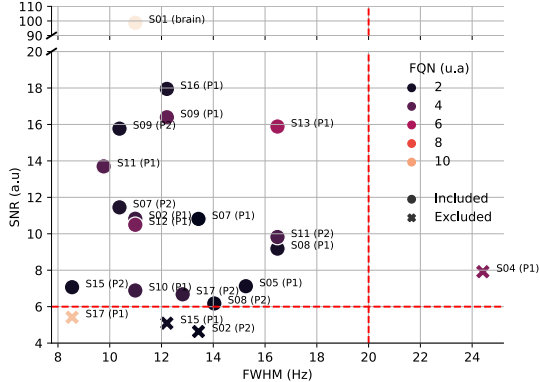


**Figure 4:** General MRS data quality of acquired semi-LASER spinal cord and brain MRS datasets at 7 T in terms of SNR and FWHM. For each dataset, the SNR estimated on the NAA peak was plotted against FWHM of the water resonance. Any dataset with a SNR below 6 (horizontal red line) or a water FWHM above 20 Hz (vertical red line) or a FQN above 10 were rejected. The SNR and FWHM of one brain MRS dataset were also plotted (S01). FWHM values were relatively consistent and found around 13 Hz (0.04 ppm) while the estimated SNR showed a large variability, between 4 and 18.

## Discussion

In this work, in-line with previous methodological developments to improve  $^1\text{H}$  spinal cord MRS robustness, a dedicated acquisition protocol, data processing and quantification method were designed at 7 T. The method particularly focuses on the dynamic  $B_0$  field heterogeneities induced by subject breathing and their mitigation using respiratory-triggered acquisition and raw data processing approaches. Promising results were obtained on a group of 14 healthy subjects.

During the past years, MR spectroscopy has benefited from great methodological improvements at UHF, in particular for brain MRS applications [11]. The development of novel RF coil designs and the continuous progress in acquisition methods have been

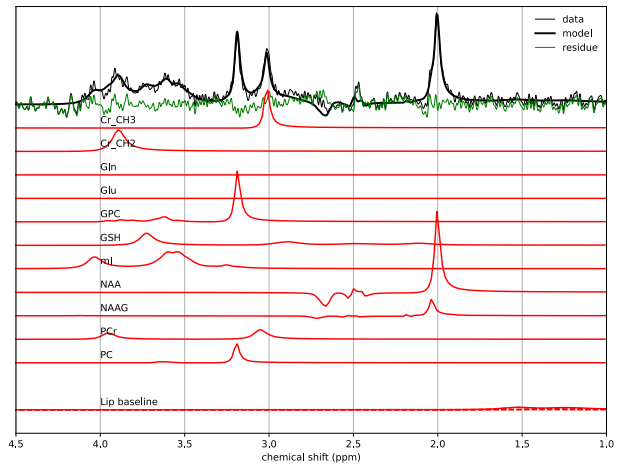


**Figure 5:** Fitting results for a MR semi-LASER spectrum (subject S09) acquired on the spinal cord at 7 T: acquired spectrum (thin black line) (post-processed), estimated spectrum (thick black line), fit residue (green) and individual metabolite spectra (red). The estimated spectrum was obtained by adjusting a parametric MRS model that consisted of a sum of metabolite spectral signatures numerically computed. The metabolite basis sets included Cr, Glu, Gln, GSH, GPC, mI, NAA, NAAG, PC and PCr. tCho, tCr and tNAA concentrations were computed by summing the concentration estimates from GPC and PC, Cr and PCr, NAA and NAAG, respectively. Note the substantial residue left in the 2-3 ppm region and at c.a. 3.8 ppm due to the misfitting of strongly coupled metabolites such as Gln, Glu and generally the low SNR available in spinal cord MRS.

converging toward the common objective of improving MRS data quality. In this study, special care was taken in evaluating the data quality in terms of SNR and FWHM (Fig. 4). The group-average SNR (11.01) was in good agreement with previous studies (Table 2); the FWHM measured in this study (0.04 ppm) was the lowest reported up to now for spinal cord MRS. Although being far from the SNR available when performing brain MRS (Fig. 1), the signal enhancement obtained in this study on spinal cord was reached likely through the successful handling of physiological motion and in particular breathing during the acquisition and data reconstruction.

Physiological events such as cardiac pulsatility and breathing constitute a major source of motion but with various indirect effects. Recently, Vannesjo et al. reported that substantial  $B_0$  field fluctuations due to breathing take place in the spinal cord at 7 T [18]. The latter was evidenced by recording the respiratory trace and comparing the time evolutions with values obtained from rapid  $B_0$  field map imaging acquisitions. Similarly in this work, these field fluctuations were measured by short-TR noWS MRS acquisitions using a voxel located at the C3 level. Assuming the water peak FWHM indirectly reflects the  $B_0$  field homogeneity within the VOI, the results obtained during normal breathing (Fig. 2) and breath-hold (Fig. S1) are in strong agreement with Vannesjo et al.'s report.

To the best of our knowledge, this is the first time that a human spinal cord MRS protocol includes respiratory-triggering. Additionally, a dedicated data processing was developed to compensate for residual breathing  $B_0$  field fluctuations. Up to now, all human spinal cord MRS reports at low, high and ultra-high fields mentioned either the use of ECG-triggering or no specific triggering mode [14, 1]. In

2013, Hock et al. investigated the use of cardiac triggering approaches for spinal cord MRS at 3 T [26]; when employed for  $B_0$  field homogenization, ECG-triggering slightly improved first-order shimming efficiency and reduced the water FWHM of 1.3 Hz (ca. 10 %) in average when compared to acquisitions performed without triggering (8 healthy subjects). In 2016, the same authors suggested a somewhat similar approach to the one presented here for motion correction at 3 T; the method relied on a retrospective gating of ECG-triggered spinal cord metabolite-cycled MRS data acquired along with three 1D axial navigators [19]. In this work, additionally to the respiratory-triggering, a fully automatic raw data processing was developed to discard individual scans that do not contribute in increasing the SNR and/or spectral resolution (Fig. 3). At group-level, an average of 6% of corrupted individual scans acquired were discarded. Moreover, similarly to previous reports [19], this post-acquisition approach was very efficient in detecting and discarding corrupted scans due to subject motion as shown in Fig. S2. Metabolite cycling (MC) MRS represents another excellent alternative for motion and  $B_0$  field fluctuations compensation as it allows the acquisition of an intense non-saturated water resonance particularly useful for data post-correction. Hock et al. reported the feasibility of MC-MRS on the human spinal cord at 3 T [19, 38, 40]. While MC-MRS was successfully reported for brain applications at UHF [41, 42, 43, 44], this preparation technique remains extremely challenging at 7 T in other organs because of its sensitivity to  $B_1^+$  field inhomogeneities, its high demand in terms of SAR, TR and thus scan time.

Considering the small size of the VOI in the spinal cord, special care was taken to homogenize the local  $B_0$  field as it is a key factor to collect high-

quality MRS data. Surprisingly, second-order shimming rarely improved the  $B_0$  field homogeneity within the VOI and increased the water FWHM of c.a. 10 Hz in average. The size of the VOI, the reduced SNR and probably the CSF-induced phase distortions likely corrupted the spatial phase profiles acquired and required for second-order  $B_0$  shimming.

## Quantification

Prior to MRS data quantification, some datasets and subjects were excluded from the study based on data and fit quality parameters. The SNR threshold (6) was adjusted arbitrarily whereas the FWHM threshold (20 Hz) was set in agreement with recent recommendations [20]. The FQN, ideally close to 1, was employed as a third threshold (10) to discard any fit exhibiting strong residue. In summary, 80% of the acquired spinal cord MRS datasets were successfully included in the study using the latter criteria. Metabolite concentration ratios were computed from the estimations obtained with the in-house developed quantification tool (Table 1), but also LCModel (Table S1). The estimation of absolute concentrations and the correction for partial volume effects were attempted but resulted in strong overestimations (data not shown). For these reasons, metabolite ratios relative to tCr were computed as it is commonly the case in spinal cord MRS [1]. The quantification SD, CRB, COV were reduced in most cases when employing data discard. In the case of tNAA, SDs dropped from 0.46 to 0.22 while the COV for tCho decreased from 15.33% to 13.21%. The concentration ratios for tCho, tNAA and mI were in very good agreement with previous high and low field spinal cord MRS reports (Table. 2), their variability in terms of SD and COV were relatively low except for mI. Inter-

estingly, GSH, a marker of cellular oxidative stress, showed relatively low variability in terms of COV. To the best of our knowledge, while inter-subjects COV are commonly reported under 30% [13, 39], no spinal cord quantitative MRS reports mention intra-subject multiple time points reproducibility tests. Metabolites ratios such as Glu and Gln were discarded from discussion due to their high CRB and/or COV (Table 1) showing that it remains extremely challenging to quantify accurately such low-concentrated coupled metabolites in the case of spinal cord MRS at 7 T. These quantification results were not significantly different and were in good agreement with the metabolite ratios estimated LCModel (Table S1).

## Limitations

While the average subject BMI was within the healthy range [20; 25], it remains relatively low (20.56) and poorly distributed ( $\pm 2.89$ ). The acquisition protocol presented in this paper could be potentially applied as it is to low BMI pathological subjects. It would need however to be adapted or even redesigned for subjects with larger BMI depending on the RF coil  $B_1$  performances.

ECG-triggering is the recommended triggering method in the spinal cord MRI literature [14, 1] and was shown as a requirement for MRS too at 3 T [8, 26]. As demonstrated in this report, respiratory-triggering can substantially improve spinal cord MRS spectral quality at 7 T. A comparative study evaluating the benefits of all triggering techniques currently available such as ECG-, respiratory and double-triggering methods, in terms of scan time, data quality and quantification accuracy would be of great interest to conclude on the optimal methodology for spinal cord MRS at UHF. The main consequences

and drawbacks of respiratory-triggering lay in its variable TR lengthening, which strongly impacts the acquisition scan time (Table. 2). Ideally, one individual MR spectrum should be acquired every breathing cycle. Considering a normal breathing rate of 12-16 BPM in adults, the minimum TR of the respiratory-triggered MRS sequence should remain below 3.75s. In this study, because of the cervical RF coil design in use and the high-B<sub>1</sub> power required, the TR was constrained to a minimum of 4.85s in average consequently extending the effective scan time. Parallel transmission (pTx) and its application to lower SAR constraints would be of great interest [45]. Moreover, respiratory-triggering like any triggered methods requires short acquisition durations. The 760-ms VAPOR scheme used in this study may thus require further optimizations, which were nonetheless not possible due to the specific semi-LASER sequence implementation.

The MRS VOI dimensions were substantially extended along the HF direction to follow the tubular spinal cord shape. While the latter practice is common and helps rising SNR, it also increases CSDE and partial volume effects. This effect in combination with strong cord curvature and CSF pulsatility can potentially corrupt the MRS acquisitions and in particular affect resonances subject to large CSDE voxel displacements (NAA and water in this study). While residual water is likely to originate from small CSF compartments such as the central canal, the anterior median fissure and the posterior median sulcus [46], previously described CSDE combined with poor spatial localization due to inhomogeneous B<sub>1</sub> field could result in the presence of residual water signals originating from the CSF around the cord.

Regarding data quantification, the fit model did not include any macromolecular resonances except

for 3 lipid components below 2 ppm that likely originated from the fat around the neck region. Indeed, the IR MRS acquisitions performed on brain using the exact same protocol as on spinal cord revealed a very low macromolecular spectral baseline. Nevertheless, these IR-MRS experiments were carried out in brain to benefit from high SNR; it would be of great interest to reproduce the latter tests on the spinal cord itself and be able to establish its specific macromolecular spectral profile.

### Conclusions and perspectives

To conclude, we demonstrated the interest of respiratory-triggered acquisition to collect robust <sup>1</sup>H MRS data from the cervical spinal cord at 7 T. A dedicated raw data processing algorithm was developed to enhance MR spectral quality by discarding corrupted scans. This processing and quantification tool has been made open source and available at (<https://crmbm.univ-amu.fr/softwares/pastis>). The methodology was tested on a cohort of 14 healthy volunteers. Common metabolite ratios such as tCho/tCr, tNAA/tCr and mI/tCr were successfully quantified. Interestingly, the careful use of first-order B<sub>0</sub> shimming allowed a high spectral resolution, better than in previous reports. GSH/tCr concentration ratio was quantified thus revealing the benefits of such breathing-triggered and processing approaches. The study additionally highlighted that the spinal cord MRS data quality was highly dependent on motion breathing, subject motion and subject BMI.

Assuming the anatomical imaging is performed, the total scan time including field homogenization adjustments would be of 18min in average. This protocol could potentially be applied, as it is, to subjects having BMI within low or normal ranges. The de-

development of novel RF coil designs in combination with pTx implementations should allow further use of such MRS methods for a larger number of spinal cord pathologies. Indeed, while many neurodegenerative diseases are studied using MR imaging, the need for a better understanding of their metabolism in the spinal cord remains crucial. This high-quality MRS data approach would be of particular relevance to assess spinal cord multiple sclerosis, amyotrophic lateral sclerosis and injury metabolism. open-source and publicly available at this address: <https://crmbm.univ-amu.fr/softwares/pastis>

## Acknowledgements

The MRS package was developed by Gülin Öz and Dinesh Deelchand (semi-LASER sequence) and provided by the University of Minnesota under a C2P agreement. This work was performed on the platform 7T-AMI, a French ‘Investissements d’Avenir’ programme (grant ANR-11-EQPX-0001). The project leading to this publication has received funding from Excellence Initiative of Aix-Marseille University – (A\*MIDEX-EI-17-29-170228-09.43-Imetionic-7), a French ‘Investissements d’Avenir’ programme, and from the Fondation pour l’Aide à la Recherche sur la Sclérose en Plaques (ARSEP). This work was performed by a laboratory member of France Life Imaging network (grant ANR-11-INBS-0006). The authors would like to thank Joevin Sourdon for beta testing the processing and quantification software and Véronique Gimenez, Claire Costes and Lauriane Pini for study logistics.

## Data availability statement

The in-house developed Python package dedicated to MRS data processing and quantification was made

## References

- [1] Wyss PO, Hock A, Kollias S. The application of human spinal cord magnetic resonance spectroscopy to clinical studies: A review. *Seminars in ultrasound, CT, and MR* 2017; 38:153–162.
- [2] Marlani AF, Clementi V, AlbiniRiccioli L, Agati R, Carpenzano M, Salvi F, Leonardi M. Quantitative cervical spinal cord 3 T proton MR spectroscopy in multiple sclerosis. *AJNR* 2010; 31:180–184.
- [3] Carew JD, Nair G, PinedaAlonso N, Usher S, Hu X, Benatar M. Magnetic resonance spectroscopy of the cervical cord in amyotrophic lateral sclerosis. Amyotrophic lateral sclerosis : official publication of the World Federation of Neurology Research Group on Motor Neuron Diseases 2011; 12:185–191.
- [4] Wyss PO, Huber E, Curt A, Kollias S, Freund P, Henning A. MR spectroscopy of the cervical spinal cord in chronic spinal cord injury. *Radiology* 2019; 291:131–138.
- [5] Lin AP. Overcoming technical challenges of MR spectroscopy in chronic spinal cord injury. *Radiology* 2019; 291:139–140.
- [6] Oz G, Deelchand DK, Wijnen JP, Mlynárik V, Xin L, Mekle R, Noeske R, Scheenen TWJ, Tkáč I. Advanced single voxel 1H magnetic resonance spectroscopy techniques in humans: Experts' consensus recommendations. *NMR Biomed* 2020; 34:e4236.
- [7] Stroman PW, WheelerKingshott C, Bacon M, Schwab JM, Bosma R, Brooks J, Cadotte D, Carlstedt T, Ciccarelli O, CohenAdad J, Curt A, Evangelou N, Fehlings MG, Filippi M, Kelley BJ, Kollias S, Mackay A, Porro CA, Smith S, Strittmatter SM, Summers P, Tracey I. The current state-of-the-art of spinal cord imaging: methods. *Neuroimage* 2014; 84:1070–1081.
- [8] Hock A, Henning A, Boesiger P, Kollias SS. 1H-MR spectroscopy in the human spinal cord. *AJNR* 2013; 34:1682–1689.
- [9] Trattnig S, Bogner W, Gruber S, Szomolanyi P, Juras V, Robinson S, Zbýň Š, Haneder S. Clinical applications at ultrahigh field (7 T). Where does it make the difference? *NMR Biomed* 2016; 29:1316–1334.
- [10] Ladd ME, Bachert P, Meyerspeer M, Moser E, Nagel AM, Norris DG, Schmitter S, Speck O, Straub S, Zaiss M. Pros and cons of ultra-high-field MRI/MRS for human application. *Prog Nucl Magn Reson Spectrosc* 2018; 109:1–50.
- [11] Henning A. Proton and multinuclear magnetic resonance spectroscopy in the human brain at ultra-high field strength: A review. *Neuroimage* 2018; 168:181–198.
- [12] de Graaf RA, ‘In Vivo NMR Spectroscopy: Principles and Techniques’. Wiley-Interscience, 3rd ed., March 2019.

- [13] Henning A, Koning W, Fuchs A, Raaijmakers A, Bluemink JJ, van den Berg CAT, Boer VO, Klomp DWJ. *1H MRS in the human spinal cord at 7 T using a dielectric waveguide transmitter, RF shimming and a high density receive array.* NMR Biomed 2016; 29:1231–1239.
- [14] Barry RL, Vannesjo SJ, By S, Gore JC, Smith SA. *Spinal cord MRI at 7 T.* NeuroImage 2018; 168:437–451.
- [15] Garwood M, DelaBarre L. *The return of the frequency sweep: designing adiabatic pulses for contemporary NMR.* J Magn Res 2001; 153:155–177.
- [16] Oz G, Tkáč I. *Short-echo, single-shot, full-intensity proton magnetic resonance spectroscopy for neurochemical profiling at 4 T: validation in the cerebellum and brainstem.* Magn Reson Med 2011; 65:901–910.
- [17] Duerst Y, Wilm BJ, Wyss M, Dietrich BE, Gross S, Schmid T, Brunner DO, Pruessmann KP. *Utility of real-time field control in T2\*-weighted head MRI at 7 T.* Magn Reson Med 2016; 76:430–439.
- [18] Vannesjo SJ, Miller KL, Clare S, Tracey I. *Spatiotemporal characterization of breathing-induced B0 field fluctuations in the cervical spinal cord at 7 T.* Neuroimage 2018; 167:191–202.
- [19] Hock A, Henning A. *Motion correction and frequency stabilization for MRS of the human spinal cord.* NMR Biomed 2016; 29:490–498.
- [20] Juchem C, Cudalbu C, de Graaf RA, Gruetter R, Henning A, Hetherington HP, Boer VO. *B0 shimming for in vivo magnetic resonance spectroscopy: Experts' consensus recommendations.* NMR Biomed 2021; 34:e4350.
- [21] Near J, Harris AD, Juchem C, Kreis R, Marjańska M, Oz G, Slotboom J, Wilson M, Gasparovic C. *Preprocessing, analysis and quantification in single-voxel magnetic resonance spectroscopy: Experts' consensus recommendations.* NMR Biomed 2021; 34:e4257.
- [22] Cudalbu C, Behar KL, Bhattacharyya PK, Bogner W, Borbath T, de Graaf RA, Gruetter R, Henning A, Juchem C, Kreis R, Lee P, Lei H, Marjańska M, Mekle R, MuraliManohar S, Považan M, Rackayová V, Simicic D, Slotboom J, Soher BJ, Starčuk Z, Starčuková J, Tkáč I, Williams S, Wilson M, Wright AM, Xin L, Mlynárik V. *Contribution of macromolecules to brain 1H MR spectra: Experts' consensus recommendations.* NMR Biomed 2021; 34:e4393.
- [23] Deelchand DK, Kantarci K, Öz G. *Improved localization, spectral quality, and repeatability with advanced MRS methodology in the clinical setting.* Magn Reson Med 2018; 79:1241–1250.
- [24] Tkac I, Starcuk Z, Choi IY, Gruetter R. *In vivo 1H NMR spectroscopy of rat brain at 1 ms echo time.* Magn Reson Med 1999; 41:649–656.

- [25] Gruetter R, Tkáč I. Field mapping without reference scan using asymmetric echo-planar techniques. *Magn Reson Med* 2000; 43:319–323.
- [26] Hock A, Fuchs A, Boesiger P, Kollias SS, Henning A. Electrocardiogram-triggered, higher order, projection-based B0 shimming allows for fast and reproducible shim convergence in spinal cord 1H MRS. *NMR Biomed* 2013; 26:329–335.
- [27] Schaller B, Xin L, Gruetter R. Is the macromolecule signal tissue-specific in healthy human brain? A 1H MRS study at 7 Tesla in the occipital lobe. *Magn Reson Med* 2014; 72:934–940.
- [28] Snoussi K, Gillen JS, Horska A, Puts NAJ, Pradhan S, Edden RAE, Barker PB. Comparison of brain gray and white matter macromolecule resonances at 3 and 7 Tesla. *Magn Reson Med* 2015; 74:607–613.
- [29] Provencher S. “LCModel and LCMgui user’s manual”. <http://www.s-provencher.com/lcm-manual.shtml>, February 2021.
- [30] Ratiney H, Sdika M, Coenradie Y, Cavassila S, van Ormondt D, GraveronDemilly D. Time-domain semi-parametric estimation based on a metabolite basis set. *NMR Biomed* 2005; 18:1–13.
- [31] Smith SA, Levante TO, Meier BH, Ernst RR. Computer simulations in magnetic resonance An object-oriented programming approach. *Journal of Magnetic Resonance, Series A* 1994; 106:75–105.
- [32] Provencher SW. Estimation of metabolite concentrations from localized in vivo proton NMR spectra. *Magn Reson Med* 1993; 30:672–679.
- [33] Marjańska M, Auerbach EJ, Valabrègue R, Van de Moortele PF, Adriany G, Garwood M. Localized 1H NMR spectroscopy in different regions of human brain in vivo at 7 T: T2 relaxation times and concentrations of cerebral metabolites. *NMR Biomed* 2012; 25:332–339.
- [34] Andreychenko A, Klomp DWJ, de Graaf RA, Luijten PR, Boer VO. In vivo GABA T2 determination with J-refocused echo time extension at 7 T. *NMR Biomed* 2013; 26:1596–1601.
- [35] Xin L, Gambarota G, Mlynárik V, Gruetter R. Proton T2 relaxation time of J-coupled cerebral metabolites in rat brain at 9.4 T. *NMR Biomed* 2008; 21:396–401.
- [36] Michaeli S, Garwood M, Zhu XH, DelaBarre L, Andersen P, Adriany G, Merkle H, Ugurbil K, Chen W. Proton T2 relaxation study of water, N-acetylaspartate, and creatine in human brain using Hahn and Carr-Purcell spin echoes at 4 T and 7 T. *Magn Reson Med* 2002; 47:629–633.
- [37] Kreis R. The trouble with quality filtering based on relative Cramér-Rao lower bounds. *Magn Reson Med* 2015; 75:15–18.

- [38] Hock A, Wilm B, Zandomeneghi G, Ampanozi G, Franckenberg S, Zoelch N, Wyss PO, DeZanche N, NordmeyerMafner J, Kraemer T, Thali M, Ernst M, Kollias S, Henning A. Neurochemical profile of the human cervical spinal cord determined by MRS. *NMR Biomed* 2016; 29:1464–1476.
- [39] Marlani AF, Clementi V, AlbiniRiccioli L, Agati R, Leonardi M. Quantitative proton magnetic resonance spectroscopy of the human cervical spinal cord at 3 Tesla. *Magn Reson Med* 2007; 57:160–163.
- [40] Hock A, MacMillan EL, Fuchs A, Kreis R, Boesiger P, Kollias SS, Henning A. Non-water-suppressed proton MR spectroscopy improves spectral quality in the human spinal cord. *Magn Reson Med* 2013; 69:1253–1260.
- [41] Giapitzakis IA, Borbath T, MuraliManohar S, Avdievich N, Henning A. Investigation of the influence of macromolecules and spline baseline in the fitting model of human brain spectra at 9.4 T. *Magn Reson Med* 2019; 81:746–758.
- [42] Giapitzakis IA, Avdievich N, Henning A. Characterization of macromolecular baseline of human brain using metabolite cycled semi-LASER at 9.4 T. *Magn Reson Med* 2018; 80:462–473.
- [43] Giapitzakis IA, Shao T, Avdievich N, Mekle R, Kreis R, Henning A. Metabolite-cycled STEAM and semi-LASER localization for MR spectroscopy of the human brain at 9.4 T. *Magn Reson Med* 2017; 79:1841–1850.
- [44] Fichtner ND, Giapitzakis IA, Avdievich N, Mekle R, Zaldivar D, Henning A, Kreis R. In vivo characterization of the downfield part of  $^1\text{H}$  MR spectra of human brain at 9.4 T: Magnetization exchange with water and relation to conventionally determined metabolite content. *Magn Reson Med* 2017; .
- [45] Massire A, Bitz AK, Boulant N, Schüller D, Wichmann T, Troalen T, Ranjeva JP, Callot V. An 8Tx/8Rx coil validation workflow toward Virtual Observation Points-based parallel transmission cervical spinal cord in vivo imaging at 7 T. In: Proc. Intl. Soc. Mag. Reson. Med. 25, Honolulu, HI, USA, 2017. p. 477.
- [46] Massire A, Rasoanandrianina H, Guye M, Callot V. Anterior fissure, central canal, posterior septum and more: New insights into the cervical spinal cord gray and white matter regional organization using T1 mapping at 7T. *NeuroImage* 2020; 205:116275.

## Supplementary figure captions

- **Figure S1:** Impact of breath-hold on the spinal cord localized MRS signal. Individual acquired spectra (A), recorded respiration trace (black) overlayed with the estimated FWHM (red, B) and chemical shift changes (blue, C). The subject S12 performed 3 short breath-holds at ca. 30, 90 and 150s. The water resonance linewidth and frequency showed substantial changes during each breath-hold.

- **Figure S2:** Results of the automatic MRS data discard algorithm applied in the case of a slight subject motion. Subject S17 was asked to slightly nod his head after accumulating 64 scans (c.a. 7min). Automatic post-analysis of the residual water resonance in each individual scan resulted in its relative amplitude (A), linewidth (B), chemical shift (C) and phase (D) time courses. Peak linewidth thresholds were automatically adjusted (red, B) and corresponding scans were discarded from the dataset (E). Most of the scans acquired after subject nodding (scan index c.a. 64) were discarded demonstrating the efficiency of the correction algorithm in detecting motion.
- **Figure S3:** Normalized SNR depends on the subject BMI ( $R=0.65$ ). Datasets which were discarded from the group are shown with a (X) marker. Normalized SNR or SNR<sub>t</sub> was calculated by taking into account the VOI size and the number of averages. Position of the voxel in the Y direction was calculated relative to the center of the magnet (see colorbar). A dependence between SNR and BMI can be observed, further explained by the position of the VOI.
- **Figure S4:** Semi-LASER brain spectra acquired (subject S19) with a TE of 30 ms and without inversion-recovery (solid line), with TE/TI = 30/950 ms (dashed-dotted lines) and TE/TI = 40/950 ms (dashed lines).
- **Figure S5:** Semi-LASER spectrum acquired on subject S03 using the protocol described in the method section. A clear artifact is visible at c.a. 5.1 ppm (\*).
- **Figure S6:** Respiratory-triggered semi-LASER sequence timing and respiratory trace recorded for subject S09. Sequence preparation, the first 100 ms and the last 720 ms of the acquisition duration are represented in orange, red and gray, respectively. Four breath cycles are represented.

## Supplementary Information

*Respiratory-gated quantitative MR spectroscopy of the human cervical spinal cord at 7 T*

Tangi Roussel, Yann Le Fur, Maxime Guye, Patrick Viout, Jean-Philippe Ranjeva, Virginie Callot

### A. Subject breathing and motion impact on spinal cord MRS

#### A.1 Breath-hold spinal cord MRS

To investigate the impact of breathing on the acquisition of a localized MRS signal originating from the spinal cord, additional experiments were carried out using a similar STEAM protocol than described in the method section. Such experiments were directly inspired from Vannesjo et al. report about the characterization of the breathing-induced  $B_0$  field fluctuations in the spinal cord at 7 T [1]. During a time period of c.a. 3 minutes, the subject S12 was asked to breath normally and perform 3 short consecutive breath-holds in inspiration. Each acquired non-WS individual spectrum was analyzed and the water resonance FWHM and chemical shift variation were estimated (Fig. S1).

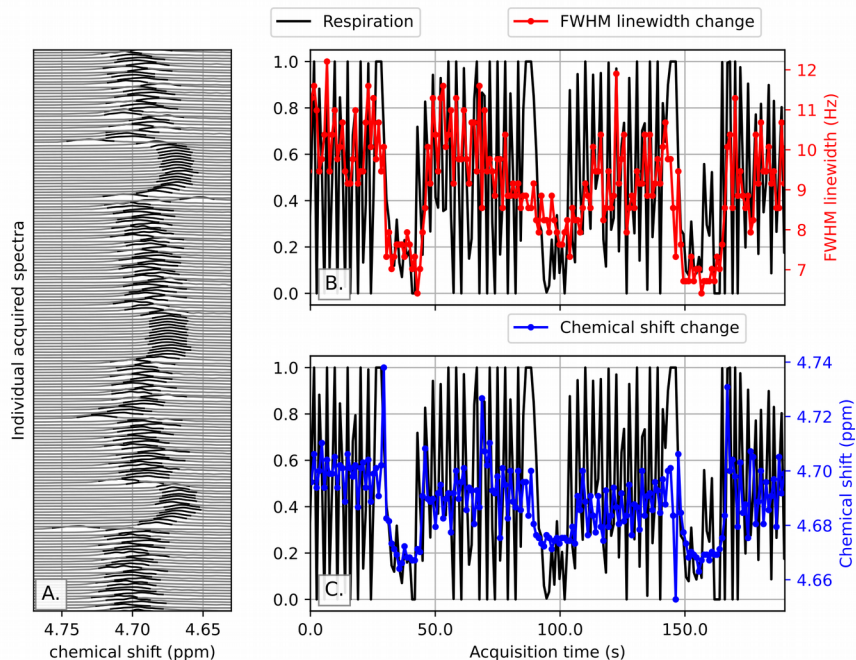


*Figure S1: Impact of breath-hold on the spinal cord localized MRS signal.*  
Individual acquired spectra (A), recorded respiration trace (black) overlaid with the estimated FWHM (red, B) and chemical shift changes (blue, C). The subject S12 performed 3 short breath-holds at ca. 30, 90 and 150s. The water resonance linewidth and frequency showed substantial changes during each breath-hold.

As already shown in Fig. 2, normal breathing impacts the water resonance linewidth and chemical shift. This effect is clearly observed in Fig. S1B and C where periodic changes in water peak linewidth and chemical shift visually correlate with the recorded respiration trace. During the

3 repeated breath-holds, the estimated water peak FWHM and chemical shift stopped oscillating and followed a time pattern that can be described as a negative rectangle function: (i) a substantial decrease, (ii) a plateau followed by (iii) an increase to its initial level. These results confirm that normal subject breathing modulates the acquired resonances' lineshape and that this effect is linked to the volume of air present in the lungs. The latter suggests that, even though the VOI is placed far from the lungs, the changes in magnetic susceptibility effects generated from the air/tissue lung interfaces are strong enough at 7 T to perturb the MR signal [1]. Note that the results obtained with the STEAM sequence are not fully representative for semi-LASER but remained the only acquisition option considering the time resolution required to observe these breathing patterns.

## A.2 Subject motion and MRS data post-correction

The automatic raw data discard algorithm developed for this study allowed an increase in the final MRS data quality observed. As described in the results section, the general increase in spectral quality was mainly due to the discard of individual spectrum showing peak linewidth distortions due to residual breathing effects. Besides physiological motion such as breathing, this post-processing method also allowed the detection of subject motion and the discard of any corrupted MRS data. To demonstrate this feature, additional acquisitions were performed on a subject using the standard semi-LASER protocol described in the method section. Without interrupting the acquisition and after averaging 64 scans, the subject (S17) was asked to slightly nod his head and then return to its initial position. Individual acquired spectra and results of the automatic data discard algorithm are shown in Fig. S2.

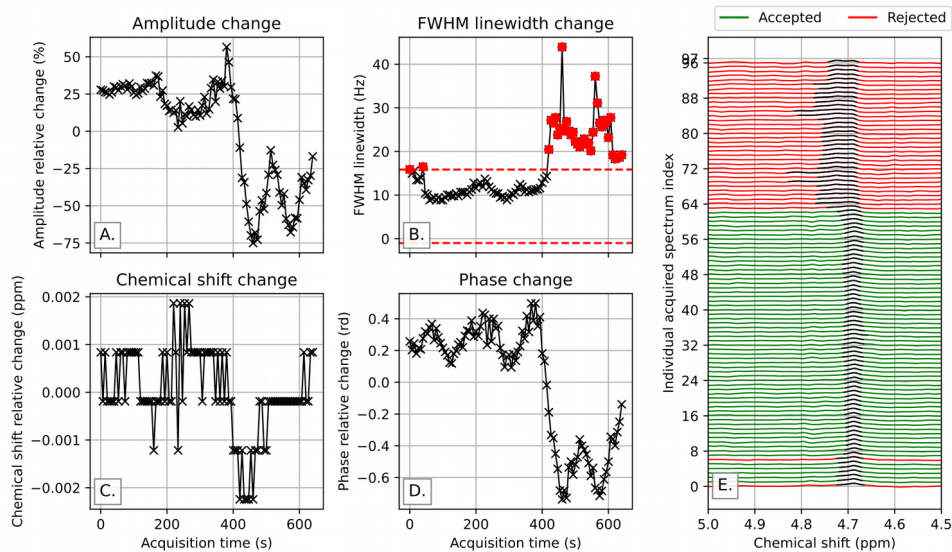


*Figure S2: Results of the automatic MRS data discard algorithm applied in the case of a slight subject motion. Subject S17 was asked to slightly nod his head after accumulating 64 scans (c.a. 7min). Automatic post-analysis of the residual water resonance in each individual scan resulted in its relative amplitude (A), linewidth (B), chemical shift (C) and phase (D) time courses. Peak linewidth thresholds were automatically adjusted (red, B) and corresponding scans were discarded from the dataset (E). Most of the scans acquired after subject nodding (scan index c.a. 64) were discarded demonstrating the efficiency of the correction algorithm in detecting motion.*

The data discard algorithm automatically adjusts thresholds to improve SNR and/or spectral resolution. These thresholds can be set in terms of peak amplitude, linewidth, chemical shift or phase. In the case of this particular experiment, the algorithm found that discarding data based on the peak linewidth estimation was the optimal method to improve the final SNR and/or decrease the final FWHM. Therefore, in this case, any individual scans showing a water peak linewidth above 17.2 Hz was discarded from the dataset (Fig. S2B). In practice, most of the data collected after the subject nodded were discarded, which shows the efficiency of this approach to post-correct MRS data for subject motion. Moreover, while the subject was asked to return his head and neck to its initial position after nodding, this analysis shows that it was likely not the case – evidencing how very slight motion can corrupt spinal cord MR acquisition in general. Note that subject motion did not only impact the MR resonances' FWHM but also their amplitude and phase, which directly reflects a VOI displacement.

## B. Normalized SNR and subject body mass index

In order to explain the high discrepancy in the MRS data quality in terms of SNR and FWHM, a correlation with multiple acquisition parameters but also with anatomical and physiological parameters were attempted. In general, the SNR of localized MRS data depends on the size of the VOI and the number of averages (NA) acquired. As discussed in the main manuscript, some of the datasets, which were actually discarded because of low SNR, were acquired with a low NA compared with the rest of the group. A “normalized SNR” was calculated by taking into account the volume of the VOI and the number of averages ( $\sqrt{NA}$ ). Interestingly, the normalized SNR depends mainly on the body mass index (BMI) of the subject and thus the voxel depth (Fig. S3).

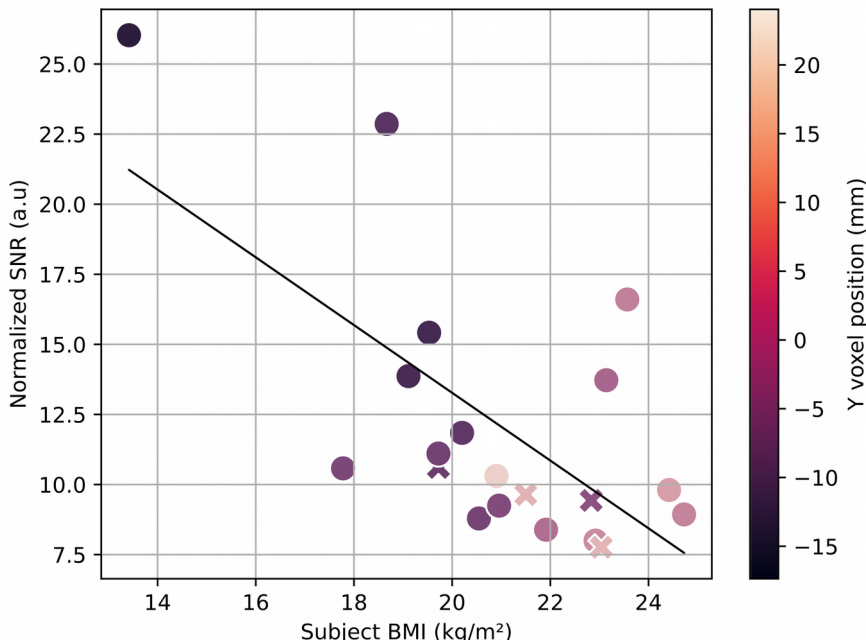
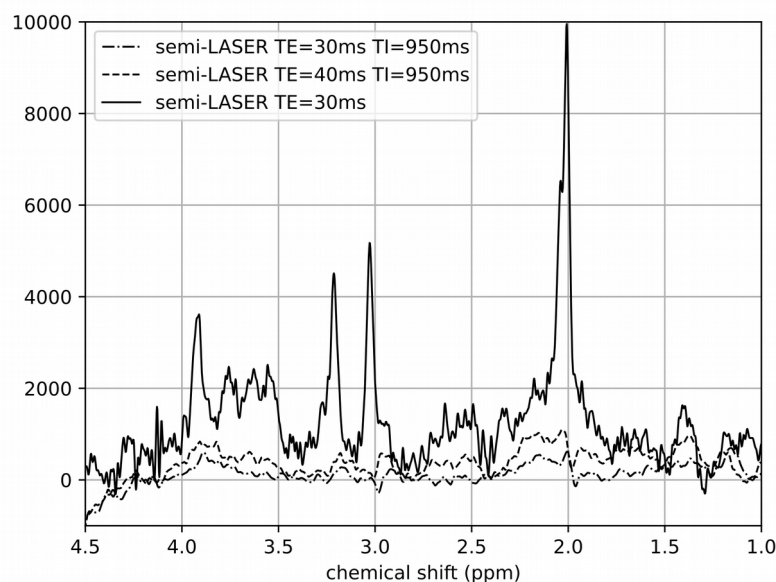


Figure S3: Normalized SNR depends on the subject BMI ( $R=0.65$ ). Datasets which were discarded from the group are shown with a (X) marker. Normalized SNR was calculated by taking into account the VOI size and the number of averages. Position of the voxel in the Y direction was calculated relative to the center of the magnet (see colorbar). A dependence between SNR and BMI can be observed, further explained by the position of the VOI.

Current product RF coils used for spine imaging at 7T are surface coils. With such design, the receive sensitivity highly depends on the distance between the coil and the VOI (Biot-Savart law). The quality of the MRS data collected in this study was impacted by this effect. Fig. S3 shows indeed (i) that the VOI position in the Y/AP direction (which reflects the spinal cord depth with regards to the RF coil) relative to the center of the magnet increased with the BMI of subjects and (ii) that the SNR decreased in high BMI subjects. A c.a. 2-fold SNR difference is observed between subjects with low (~18) and high BMI (~25). The discrepancy of the MRS data quality in this study cannot be explained only based on subject BMI. This analysis reveals however that subject BMI could be a parameter to take into account when designing the MRS protocol.

### C. Inversion-recovery MRS brain spectra

As recently suggested by Cudalbu et al. [2], inversion recovery (IR) semi-LASER acquisitions were performed to evaluate the presence and potentially model macromolecular (MM) resonances. However, IR-MRS experiments are prone to very low SNR and require substantial acquisition times. Making the simplistic assumption that the macromolecular baseline distribution is similar in the brain and in the spinal cord, these experiments were thus carried out in human brain on one subject using the protocol described in the method section. The VOI was placed in the corona radiata brain area and its volume was adjusted to 3.38 mL. 128 averages were collected using an inversion of 950 ms as suggested in literature [3,4]. The IR acquisitions were carried out for a TE of 30 and 40 ms corresponding to the shortest range of TEs employed for spinal cord MRS. IR and non-IR MRS spectra were reconstructed and denoized using a 20-Hz and 5-Hz exponential decay window, respectively (Fig. S4).



*Figure S4: Semi-LASER brain spectra acquired (subject S19) with a TE of 30 ms and without inversion-recovery (solid line), with TE/TI = 30/950 ms (dashed-dotted lines) and TE/TI = 40/950 ms (dashed lines).*

MM resonances were detected in the brain at c.a. 2.2, 2.8, 3.2 and 3.8 ppm with low signal intensities. In agreement with literature, these peaks exhibit short  $T_2$ s as shown by the intensity

drops between spectra acquired at TE=30 and 40 ms.

Recent reviews strongly recommend the acquisition and the modelization of the MM spectral baseline when performing  $^1\text{H}$  brain MRS [2,5]. In our case, considering the average low SNR (11) obtained on spinal cord MRS data compared to brain (c.a. 100), the modelization of such MM baseline would result in signal intensities far below noise level.

More generally, the MM MR spectrum depends on the brain region and significant differences have been reported between white and gray matter [2,4]. To the best of our knowledge, no exploration of the spinal cord MM profile has been performed up to now. While the use of MM a priori obtained from brain data to quantify spinal cord MRS data is tempting, it would remain only a vague approximation and could potentially generate strong metabolite fitting biases. For all these reasons, the modelization of macromolecular resonances was neglected except for 3 lipid peaks at 0.9, 1.3 and 1.6 ppm.

## D. Common downfield MRS artifact

Three spinal cord MRS datasets acquired on subjects S03, S10 and S14 showed an artifact consisting of a large resonance appearing between 5 and 5.5 ppm (Fig. S5). While this artifact is located in the downfield spectral range, its intensity and bandwidth can be so large that it can affect the resonances of interest in the upfield spectrum. When observed, its presence was associated with poor MR spectrum quality (low SNR and increased linewidth).

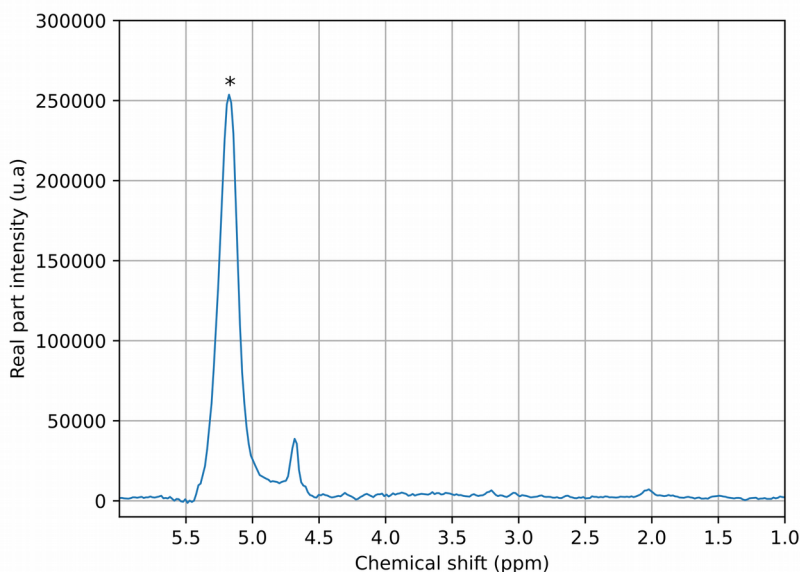


Figure S5: Semi-LASER spectrum acquired on subject S03 using the protocol described in the method section. A clear artifact is visible at c.a. 5.1 ppm (\*).

The origin of this artifact remains unclear and, to the best of our knowledge, was not documented in the literature [6]. When present in the spectrum, its intensity is stronger than any metabolite resonances and, in some cases, stronger than the residual water peak. The latter suggests that this

artifact originates from poorly saturated water protons present outside of the VOI. In summary, based on our observations in this study, the presence of this artifact was linked to a specific acquisition configuration which included: (i) very high or maximum 2<sup>nd</sup> order  $B_0$  shim voltages after attempting to perform 2<sup>nd</sup> order shimming, (ii) a VOI relatively far from the RF coil (compared to other subjects) and (iii) a relatively small VOI. Careful review of the shimming voltages before acquisition should be taken to avoid the presence of such artifact.

## E. LCModel quantification results

To evaluate the robustness of the in-house MRS quantification tool developed in this study, all datasets were additionnally quantified using LCModel [7]. Early 2021, LCModel was made free and open-source by its authors and is currently available on S. Provencher's website<sup>1</sup>. Default parameters were set<sup>2</sup> and the metabolite simulated spectrum basis file was selected according to the TE of the dataset to fit. The total choline (tCho), total creatine (tCr) and total NAA (tNAA) concentrations were computed by summing the concentration estimates from GPC and PC, Cr and PCr, NAA and NAAG, respectively. Metabolites ratios relative to tCr were computed (Table S1).

	Ratio (SD)	CRB (%)	COV (%)
<b>Gln</b>	0.71 (0.66)	72.92	41.20
<b>Glu</b>	0.60 (0.65)	174.29	122.75
<b>GSH</b>	0.39 (0.31)	122.57	54.21
<b>mI</b>	0.88 (0.56)	31.64	36.04
<b>tCho</b>	0.33 (0.15)	22.63	25.19
<b>tNAA</b>	1.62 (0.53)	22.23	8.01

*Table S1: Quantification results obtained using LCModel over 12 healthy subjects. Metabolite ratios and standard deviations (SD) were calculated. Coefficient of variation (COV) over 4 subjects (2 time points) were computed as well.*

The metabolite ratios obtained with LCModel were not significantly different ( $p>0.1$ ) from the ratios obtained with the in-house quantification software (Tables 1 and S1) except potentially for tNAA ( $p=0.02$ ).

## F. Respiratory-trigger parameters

As mentioned in the article, the respiratory trigger was set to occur during the expiratory phase. Each respiratory cycle allowed the acquisition of one single average or individual spectrum. The semi-LASER sequence timing consisted of a preparation time of 760 ms, an average TE of 46 ms and an acquisition duration of 820 ms. Note that the acquired FID signal lasted only c.a. 100 ms. The respiratory trace of subject S09 was analyzed and the previously described sequence timing was plotted for each trigger time point.

1 LCModel website: <http://s-provencher.com/lcmodel.shtml>

2 LCModel manual: <http://s-provencher.com/pub/LCModel/manual/manual.pdf>

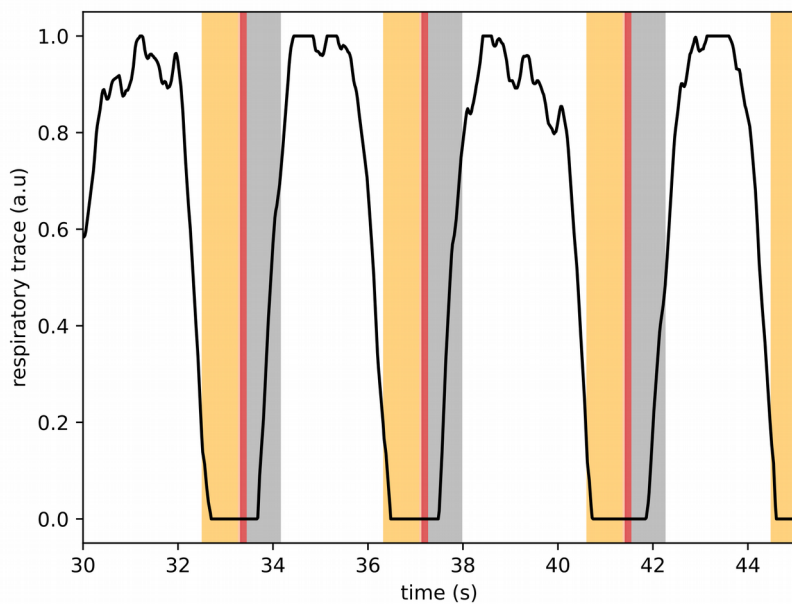


*Figure S6: Respiratory-triggered semi-LASER sequence timing and respiratory trace recorded for subject S09. Sequence preparation, the first 100 ms and the last 720 ms of the acquisition duration are represented in orange, red and gray, respectively. Four breath cycles are represented.*

As shown in figure S6, the sequence preparation, the echo time and the FID acquisition are all taking place during the expiratory pause, between two respirations.

## References

1. Vannesjo SJ, Miller KL, Clare S et al. Spatiotemporal characterization of breathing-induced B0 field fluctuations in the cervical spinal cord at 7 T Neuroimage 2018;167:191-202 doi: 10.1016/j.neuroimage.2017.11.031.
2. Cudalbu C, Behar KL, Bhattacharyya PK et al. Contribution of macromolecules to brain 1H MR spectra: Experts' consensus recommendations. NMR Biomed 2021;34:e4393 doi: 10.1002/nbm.4393.
3. Schaller B, Xin L, Gruetter R. Is the macromolecule signal tissue-specific in healthy human brain? A 1H MRS study at 7 Tesla in the occipital lobe Magn Reson Med 2014;72:934-940 doi: 10.1002/mrm.24995.
4. Snoussi K, Gillen JS, Horska A et al. Comparison of brain gray and white matter macromolecule resonances at 3 and 7 Tesla Magn Reson Med 2015;74:607-613 doi: 10.1002/mrm.25468.
5. Near J, Harris AD, Juchem C et al. Preprocessing, analysis and quantification in single-voxel magnetic resonance spectroscopy: Experts' consensus recommendations. NMR Biomed 2021;34:e4257 doi: 10.1002/nbm.4257.

6. Kreis R. Issues of spectral quality in clinical 1H-magnetic resonance spectroscopy and a gallery of artifacts NMR Biomed 2004;17:361-381 doi: 10.1002/nbm.891.

7. Provencher SW. A constrained regularization method for inverting data represented by linear algebraic or integral equations Comput Phys Commun 1982;27:213-227 doi: 10.1016/0010-4655(82)90173-4.